NANOSYSTEMS

A. GORIACHKO,[1] A. SHCHYRBA,[1,2] P.V. MELNIK,[1] M.G. NAKHODKIN[1]

[1] Faculty of Radiophysics, Taras Shevchenko National University of Kyiv
  (4g, Glushkova Ave., Kyiv 03022, Ukraine; e-mail: andreandy2000@gmail.com)
[2] Department of Physics, University of Basel
  (4056 Basel, Switzerland)

PACS 68.55.-a, 81.15.Aa,
68.37.Ef

BISMUTH GROWTH ON Ge(111): EVOLUTION OF MORPHOLOGICAL CHANGES FROM NANOCRYSTALS TO FILMS

The growth of ultra-thin bismuth films up to 15 atomic layers on the atomically clean Ge(111)-$c(2 \times 8)$ substrate at 300 K is investigated before and after the annealing at 450 K by means of ultra-high vacuum scanning tunneling microscopy. The whole range of morphologies is observed for the Bi adsorbate such as individual atoms, two-dimensional nanoislands, three-dimensional nanocrystals and microcrystals, as well as an atomically flat film. The 3D nanostructuring is achieved through the Vollmer–Weber growth mode up to 10 atomic layers, followed by film's flattening from 10 to 15 atomic layers. Annealed submonolayer films display individual Bi atoms incorporated into the uppermost atomic layer of Ge(111), as well as two-dimensional nanoislands of the first layer (2D nanostructuring). Thicker films display the coarsening after the annealing, compared to the as-deposited specimen, containing a diversity from nano- to microcrystals of bismuth.

K e y w o r d s: bismuth, germanium, thin film growth, scanning tunneling microscopy.

1. Introduction

The surfaces of bismuth (Bi) are attracting attention of the research community due to their electronic properties, being remarkably different from those of the bulk of this material [1]. Interesting spin-dependent physics (Rashba effect) was discovered both on the surface of bulk Bi crystals [2, 3] and single monolayer (1 ML) Bi films on Si(111) [4] and Ge(111) [5], while a sub-surface spin polarization reaching into the semiconductor substrate is also present in the latter case [6]. Moreover, the ultrathin Bi films have an advantage of the tunable (metallic or semiconducting) electronic properties, if their thickness is varied around the value of 1 ML [7]. Potentially, this allows one to use this substrate as a model system for the study of adsorbate properties, e.g., tuning the electronic and magnetic properties of molec-

ular layers via the intermixing of HOMO/LUMO with unoccupied/occupied electronic states of the substrate or the investigation of the surface transeffect [8, 9].

In terms of the exciting physical properties outlined above, the nanostructural aspect of ultrathin Bi films becomes increasingly important for perspective applications in nanoelectronics. To our knowledge, there is no comprehensive microscopy study of the nanostructuring in the Bi/Ge(111) system reported in the literature, in contrast to closely related systems: Bi/Si(111) [10–12], Bi/Si(001) [13–16], and Bi/Ge(001) [17]. In the previous work, we have investigated Bi on Ge(111) in the range from 0.05 to 1.5 ML [7]. A consensus appears to be existing about the equilibrium structure of 1 ML Bi on Ge(111) [7, 18, 19]. However, only the fragmentary results on the growth of more than 1.5 ML of Bi on Ge(111) obtained with real space techniques exist in the literature [20]. In the latter work, one

can find the contradictory claims concerning the incorporation of Bi atoms into the uppermost layer of Ge atoms.

The goal of the present work was to investigate the film growth in the Bi/Ge(111) system up to 15 ML at 300 K in a systematic manner by means of scanning tunneling microscopy (STM) and to find the growth regimes leading to the effective nanostructuring of a film. Another goal was a systematic study of the 450-K annealing effects on the as-deposited films, in particular, changes in films' nanostructuring and the incorporation of Bi atoms into the Ge substrate.
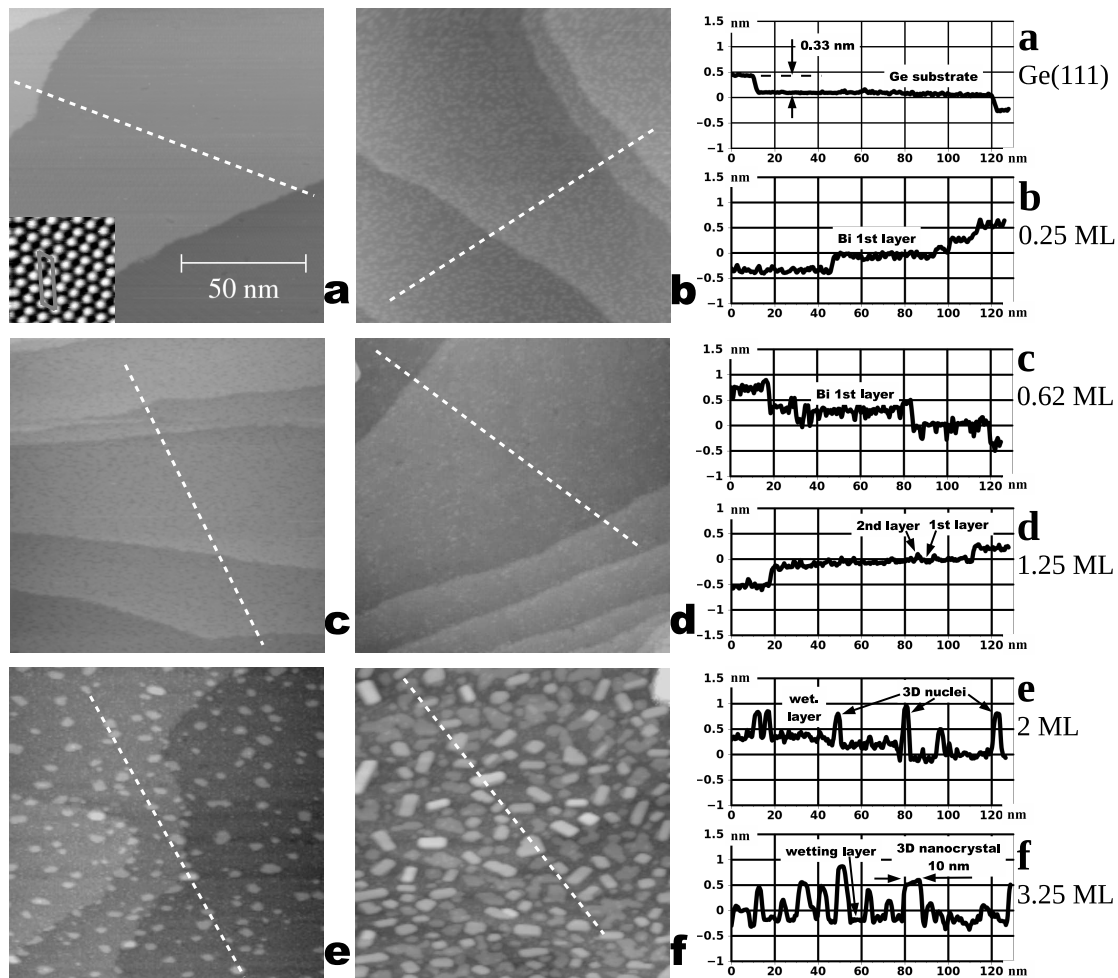
2. Experimental Part

The films were grown and investigated in an ultrahigh vacuum (UHV) chamber with a base pressure of 2×10^{-10} mbar, equipped with a home-built STM [21] and Auger electron spectrometer. The atomically clean Ge(111)-c(2×8) reconstructed surface was prepared by repeated cycles of the 500-eV Ar$^+$ bombardment at 300K and the annealing at 900 K. Bismuth was evaporated (typical rate $\sim$1 ML/min) onto the substrate from a tungsten loop, which was heated directly by the electric current, and its quantity monitored by a quartz microbalance. 1 ML is defined as the density of atoms on the bulk terminated Ge(111) surface (7.22×10^{14} atoms/cm^2). The amount of adsorbed bismuth and the cleanness of the surface was monitored by Auger electron spectroscopy (AES).

STM images were obtained in the constant current mode (typical tunneling current of 0.3 nA). Probe tips were made of a platinum-iridium wire (80% Pt, 20% Ir) by means of the simple mechanical cutting, followed by the electron bombardment in UHV with 2.5-kV voltage applied between the tip and the cathode. In several cases, we have used atomic force microscopy (AFM) in order to investigate the morphology of annealed films on the micrometer scale *ex-situ*. The AFM investigations were performed in the non-contact mode on the NT-MDT SMENA system under ambient conditions. It was equipped with silicon cantilevers characterized by resonant frequencies in the range between 100 kHz and 200 kHz, terminated by tips with apex of the curvature radius equal to 10 nm. All STM and AFM images were obtained at room temperature (RT).

3. Morphology and Structure
of as-Grown Bi Films on Ge(111)-c(2×8)

We present the STM investigations of the morphology of Bi films as a function of the Bi coverage (θ_{Bi}) deposited onto the atomically clean Ge(111)-c(2×8) substrate, which was kept at RT, $\sim$300 K. For the easier comparison, all STM images in Figs. 1–2 are plotted on identical grey scales, where brighter regions are higher, and darker regions are lower, the full span from black to white corresponds to the 2.7 nm height difference. In a similar manner, all height-distance cross-sections, found in the right-most column of Figs. 1–2, are plotted on identical scales both in horizontal and vertical directions. However, only the height differences can be compared, since these cross-sections do not share any common reference point. Figure 1 demonstrates the first growth stage, namely the transition from the atomically clean substrate to a highly nanostructured Bi film. Figure 1, *a* shows the typical state of atomically clean Ge(111)-c(2×8) prior to any bismuth deposition. In this state, the surface consists of atomically flat terraces separated by single monoatomic steps, whose height agrees well with the known $\sim$0.33 nm separation between neighboring bilayers along the [111] direction in the Ge bulk. Atomic resolution images of smaller areas amidst the terraces have shown a high quality c(2×8) reconstruction (e.g., the inset in the lower left corner of Fig. 11, *a*), which is the ground state of the Ge(111) surface, as known in the literature [22–25].

The initial stages of the Bi film growth were thoroughly investigated in our previous work [7]. These growth stages correspond to Fig. 1, *b–d* with a homogeneous coverage of Ge terraces by $\theta_{Bi} = 0.25$ ML (Fig. 1, *b*), 0.62 ML (Fig. 1, *c*), and 1.25 ML (Fig. 1, *d*). In this way, a wetting layer of bismuth is formed on the germanium substrate. At $\theta_{Bi} = 2$ ML, the three-dimensional (3D) islands up to 1 nm in height can be clearly seen in Fig. 1, *e* above the wetting layer bacground. At this point, it may seem that the growth mode of the Bi film is Stranski–Krastanov, but this is due to the lack of a detalization within the large-scale STM images. Later on, we will demonstrate that such conclusion is not correct in a very strict sense. In Fig. 1, *f*, the film has grown further to $\theta_{Bi} = 3.25$ ML, and the former 3D nuclei have developed into well-pronounced nanocrystals of the predominantly rec-
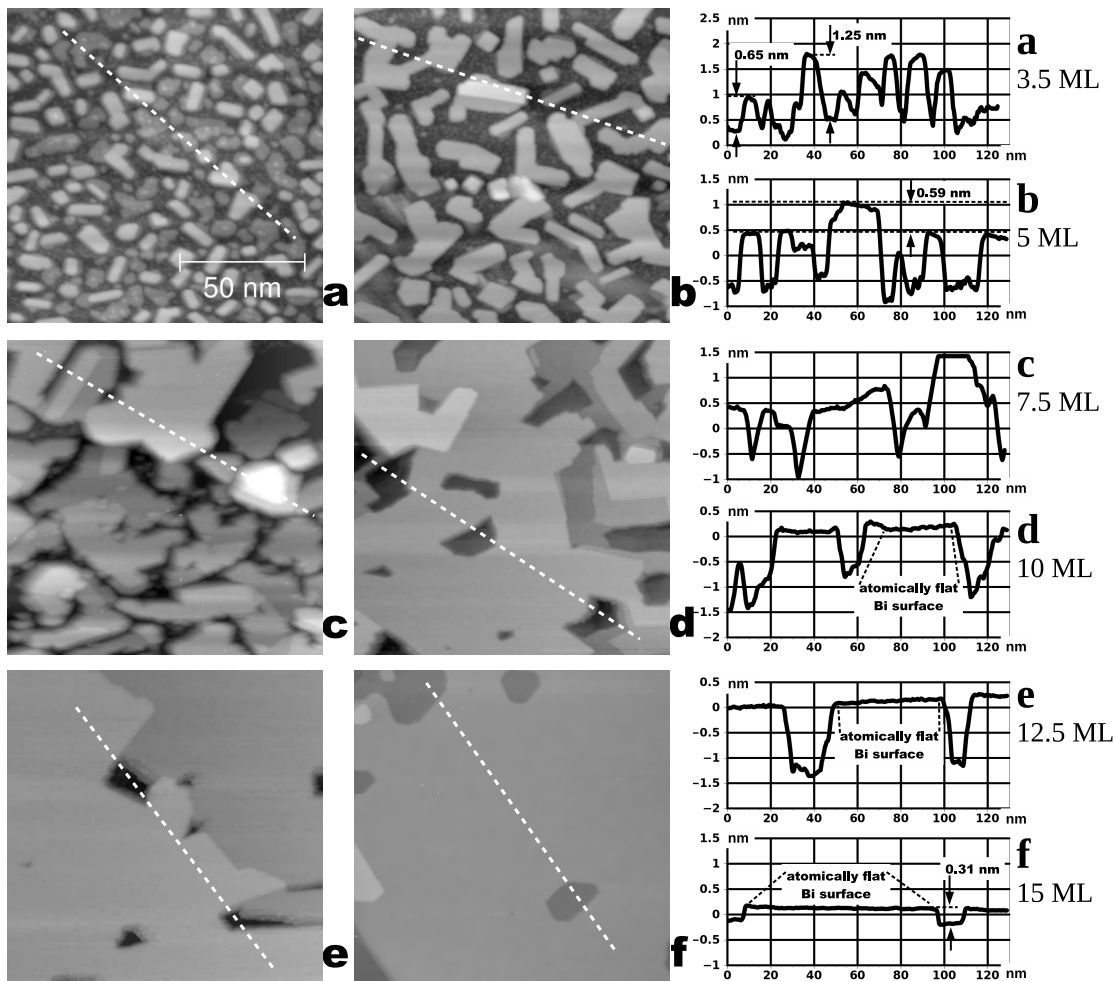
Fig. 1. Growth stage I: From the atomically flat Ge(111)-c(2 × 8) substrate to a nanocrystalline Bi film. All STM images are 125 nm × 125 nm, specimen bias voltages are: *a)* +1 V; *b)* +2.5 V; *c)* −2 V; *d)* −2 V; *e)* +1 V; *f)* +2 V. The full grey-scale range corresponds to the 2.7 nm height difference between black and white. The right-most column contains cross-sections, which were obtained as height vs distance curves along white dashed lines within corresponding images. Every cross-section is labeled by the same letter as the image, in which it was taken, and by the deposited amount of Bi (in monolayers). Different cross-sections do not share any common height reference point, only the height differences can be compared. The inset in (*a*) is the atomic resolution image, showing a representative 6 nm × 6 nm area on the top of the atomically flat terrace, with the c(2 × 8) unit cell outlined in grey. See the text for the discussion

tangular shape (maximum lateral size of the order of 10 nm).

For the given coverage, the Bi nanocrystals are still distinct entities on the top of the wetting layer. The texture of the wetting layer is similar in both cases of Fig. 1, *e–f*, and so are the 3D islands' maximum heights of roughly 1 nm above it. From this follows the lateral growth of the already formed 3D nuclei after the deposition of the additional material on the

specimen. In Fig. 2, *a*, the $\theta_{Bi} = 3.5$ ML is just slightly higher than $\theta_{Bi} = 3.25$ ML of Fig. 1, *f*, thus guiding the reader continuously between the growth stages. At this point, we observe Bi nanocrystals on the background of the wetting layer, the latter consisting of irregular Bi clusters up to several nm in size. The heights of nanocrystals' upper facets relative to the wetting layer appear to be fixed at values equal to 0.65 nm and 1.25 nm.

Fig. 2. Growth stage II: From the nanocrystalline to atomically flat Bi film. All STM images are 125 nm × 125 nm, specimen bias voltages are: *a*) +2 V; *b*) −1 V; *c*) −0.5 V; *d*) +0.1 V; *e*) +0.1 V; *f*) −2 V. The full grey-scale range corresponds to the 2.7 nm height difference between black and white. The right-most column contains cross-sections, which were obtained as height vs distance curves along white dashed lines within corresponding images. Every cross-section is labeled by the same letter as the image, in which it was taken, and by the deposited amount of Bi (in monolayers). Different cross-sections do not share any common height reference point, only the height differences can be compared. See the text for the discussion

Next, we observe a transition from an array of individual Bi nanocrystals to a continuous and atomically flat film. It starts with a dramatic increase of nanocrystals' lateral sizes, reaching several dozen nm laterally for $\theta_{Bi} = 5$ ML in Fig. 2, *b*, which is much bigger than in Fig. 2, *a*. These nanocrystals have extended straight line borders indicating a substantial transport of the deposited material during the coalescence of arbitrarily oriented small nanocrystals of Fig. 2, *a* into larger ones. The nanocrystals have atomically flat upper facets at heights differing by a discrete value of 0.59 nm. At $\theta_{Bi} = 7.5$ ML, (Fig. 2, *c*), the nanocrystals are no longer isolated entities on the wetting layer top, instead their lateral sizes grow up to the point, where they start to touch each other, there are only small patches remaining on the surface, where the wetting layer is still visible.

The last stage of growth, which was studied in this work, is a flattening of the continuous film. In Fig. 2, *d*, at $\theta_{Bi} = 10$ ML, the film is already continuous, and no individual nanocrystals can be identified by the visual inspection of the STM image. In Fig. 2, *d*–

f, we observe the tendency of film's surface flattening as the coverage is increased from $\theta_{Bi} = 10$ ML to $\theta_{Bi} = 12.5$ ML in Fig. 2, *e* and up to $\theta_{Bi} = 15$ ML in Fig. 2, *f*. In the latter case, the surface is atomically flat, which means that it consists of atomically flat terraces separated by single atomic steps of ~ 0.31 nm in height.

The data on the Bi growth on Ge(111)-c(2 × 8) presented above are lacking the atomic-scale details. Therefore, in Fig. 3, we present STM images of higher spatial resolution, which were obtained on smaller areas than in Figs. 1–2 (25 nm × 25 nm). The grey scale was individually adjusted for every panel of Fig. 3 in order to emphasize the structure of different films in the best possible way. In a similar manner, the cross-sections in Fig. 3 are plotted with different vertical scales, since the surface roughnesses were very different for the cases in Fig. 3, *a–h*). In the empty states of the STM image of Fig. 3, *a*, at $\theta_{Bi} = 0.05$ ML, we observe individual Bi atoms (grouped into pairs in several cases) as bright spots on the background of germanium substrate's atomic structure. All Bi atoms are of the same brightness/height, corresponding to the first layer of the Bi film. In Fig. 3, *b*, at $\theta_{Bi} = 0.5$ ML, we observe three brightness/height levels in the occupied states: Ge substrate, Bi atoms of the first film's layer in clear majority, and a small number of second-layer Bi atoms. Thus, the second layer starts to nucleate before the first layer is 100% complete, which is an explicit indication that the growth mode is, strictly speaking, not Stranski–Krastanov, but the Vollmer–Weber type of growth. In Fig. 3, *c*, where $\theta_{Bi} = 1.5$ ML, four brightness levels can be recognized, corresponding to the heights of: the bare germanium substrate (very small fraction of the surface area), as well as the first, second, and third layers of Bi atoms. The second-layer islands of irregular shapes and lateral sizes of several nm are seen on the background of the first layer, while some Bi atoms are observed on the top of these islands.

The second atomically flat layer is never completed during the Bi growth on Ge(111)-c(2 × 8) at RT, as can be judged from the STM images in Fig. 3, *d–f*. At nominal $\theta_{Bi} = 2$ ML (Fig. 3, *d*), most of the surface is covered by small clusters up to a couple nm in size. These 3D clusters together with the first atomically flat monolayer of Bi atoms can be considered as the wetting layer in terms of the fil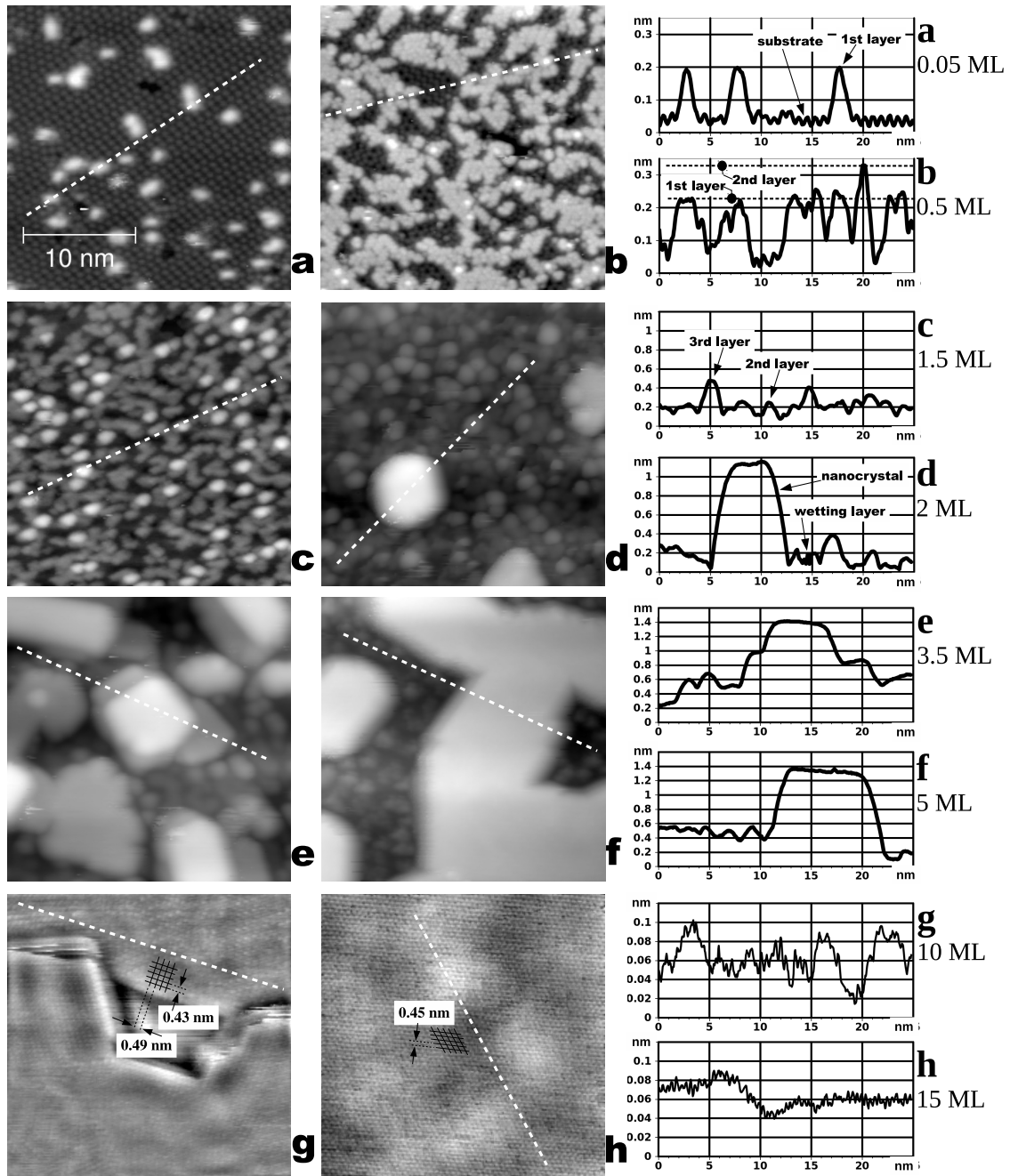m growth process. In addition, in Fig. 3, *d* and in Fig. 3, *e* ($\theta_{Bi} = 3.5$ ML), we observe nanocrystals, which are up to 1 nm higher than the wetting layer in their surrounding. The further increase of the Bi coverage leads to nanocrystals of larger lateral sizes ($\theta_{Bi} = 5$ ML, Fig. 3, *f*) and the flattening of film's surface (Figs. 3, *g–h*).

Starting from $\theta_{Bi} = 10$ ML (Fig. 3, *g*), there are extended atomically flat terraces on film's surface, which allowed one to obtain STM images with atomic resolution. In Fig. 3, *g*, one can identify a rectangular lattice with lateral periodicities of ~ 0.49 nm and ~ 0.43 nm in orthogonal directions. In Fig. 3, *h*, with $\theta_{Bi} = 15$ ML, we observe a triangular lattice with ~ 0.45 nm in-plane periodicity.
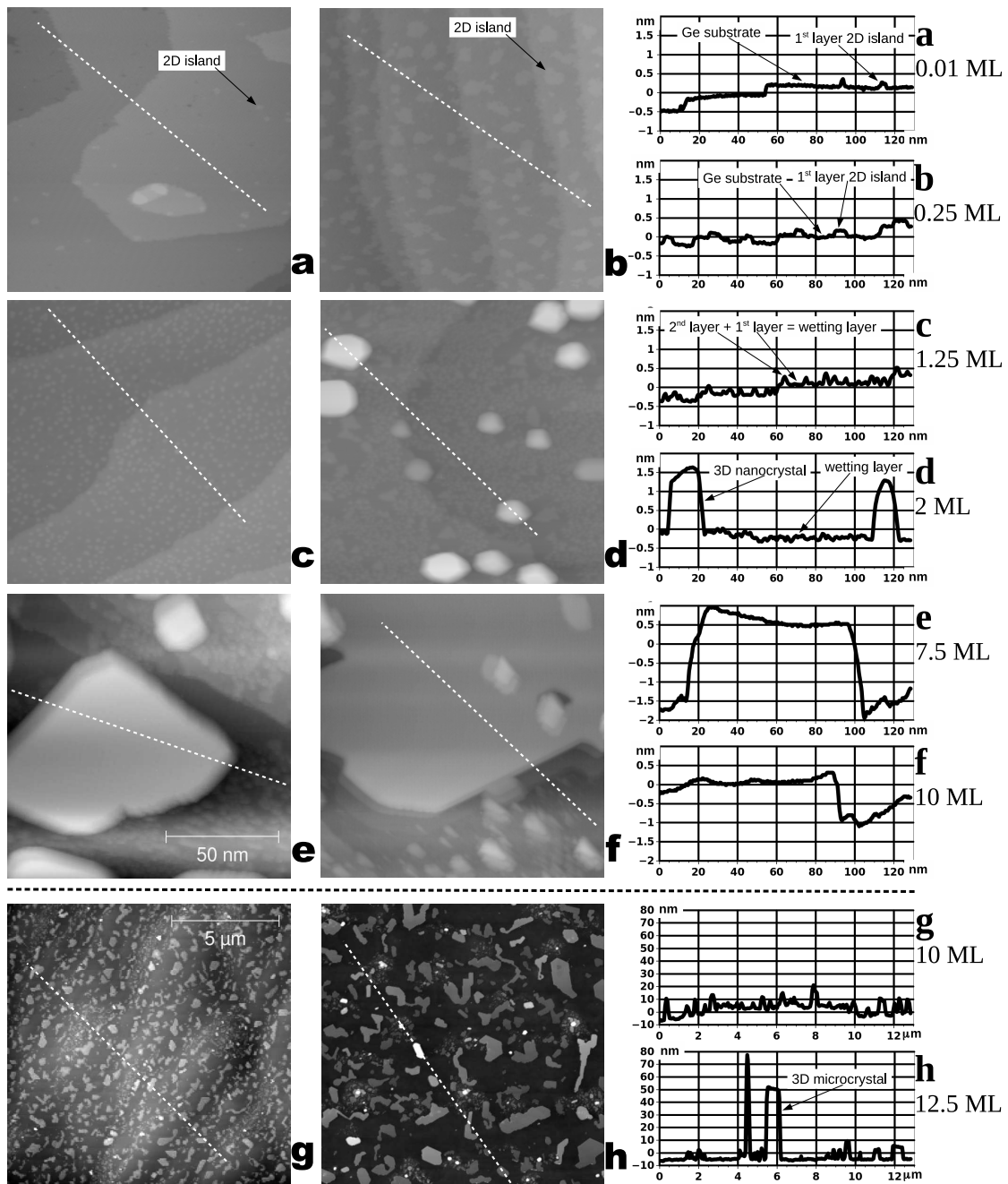
4. Modification of Film's Morphology under Thermal Stimuli

We have investigated the effects of the annealing at 450 K under the UHV conditions on the Bi films of various thicknesses after they were deposited on Ge(111)-c(2 × 8) at RT. Initially, we used STM to investigate the morphology of film's surface after the annealing for 30 min and the cooling to RT. The corresponding STM images in Fig. 4, *a–f* are plotted on the identical grey scale spanning 4.7 nm from black to white. However, they do not share any common reference height point. In Fig. 4, *a*, the specimen with $\theta_{Bi} = 0.01$ ML exhibits atomically flat terraces with very few 2D islands, which are several nm in lateral size. In Fig. 4, *b* ($\theta_{Bi} = 0.25$ ML), the surface is uniformly covered by two-dimensional (2D) islands up to a dozen nm in width. In this case, clearly, the 2D nanostructuring of the surface is achieved, as compared to the 3D nanostructuring in Figs. 1, *f*, 2, *a*, 2, *b*. The 2D nanostructures are flat islands of the first-layer Bi atoms on the top of the germanium substrate. In Fig. 4, *c*, ($\theta_{Bi} = 1.25$ ML), we observe small islands of the second layer on the uniform background of the first atomic layer of the film. In this way, the wetting layer is formed in the case of annealed films, in full agreement with our previous investigation [7], where the structure of such layer was investigated in detail.

Similar to as-deposited films, the atomically flat second layer of the annealed Bi film is never completed. Instead, in Fig. 4, *d* at $\theta_{Bi} = 2$ ML, there are already some 3D nanocrystals, which protrude up to ~ 1.7 nm above the wetting layer. As can be

Fig. 3. Bi film growth on Ge(111)-c(2 × 8) on atomic scale. All STM images are 25 nm × 25 nm, specimen bias voltages are: *a)* +2.5 V; *b)* −2 V; *c)* −2 V; *d)* −2.5 V; *e)* +2 V; *f)* −1 V; *g)* +0.05 V; *h)* +0.01 V. The right-most column contains the cross-sections, which were obtained as height vs distance curves along white dashed lines within corresponding images. Every cross-section is labeled by the same letter as the image, in which it was taken, and by the deposited amount of Bi (in monolayers). Different cross-sections do not share any common height reference point and are plotted with different height scales. *a–d)* formation of the wetting layer; *d)* nucleation of nanocrystals; *e–f)* growth and coarsening of nanocrystals; *g–h)* transition to a continuous film and the surface flattening

2D island

2D island

2D island

Ge substrate — 1st layer 2D island **a**
0.01 ML

Ge substrate – 1st layer 2D island **b**
0.25 ML

2nd layer + 1st layer = wetting layer **c**
1.25 ML

3D nanocrystal — wetting layer **d**
2 ML

e
7.5 ML

f
10 ML

50 nm **e**

f

5 μm

g
10 ML

3D microcrystal **h**
12.5 ML

g

h

Fig. 4. Bi/Ge(111) system after the annealing at 450 K: from nano- to microstructured films. In *a–g*), the specimens were annealed for 30 min; while in *h*) for 2 h. *a–f*) STM images 125 nm × 125 nm, the full grey-scale range corresponds to the 4.7 nm height difference between black and white, specimen bias voltages are: *a*) +2 V; *b*) +2 V; *c*) +2.5 V; *d*) +2 V; *e*) +1 V; *f*) +2 V. *g–h*) AFM images 12 μm × 12 μm, the full grey-scale range corresponds to the 40 nm height difference between black and white. The right-most column contains cross-sections, which were obtained as the height vs distance curves along white dashed lines within corresponding images. Every cross-section is labeled by the same letter as the image, in which it was taken, and by the deposited amount of Bi (in monolayers). Different cross-sections do not share any common height reference point, only the height differences can be compared. See the text for the discussion

recognized from Fig. 4, *d–f*, the lateral size of the largest nanocrystals within the annealed film grows dramatically with the coverage. In Fig. 4, *d*, it is up to 20 nm. While, in Fig. 4, *e* at θ_{Bi} = 7.5 ML, it is already up to 100 nm. In Fig. 4, *f*, where θ_{Bi} = 10 ML, the nanocrystals found on the surface are substantially larger than the 125 nm × 125 nm image size.

In order to adequately characterize such annealed specimens, we have obtained *ex-situ* AFM images with the field of view two orders of magnitude larger than in Fig. 4, *a–f*. The AFM images in Fig. 4, *g–h* are 12 μm × 12 μm in lateral size and are plotted on the grey-scale range of the 40 nm height difference between black and white, which is also much larger than for Fig. 4, *a–f*. Figure 4, *g* was obtained for the same specimen as Fig. 4, *f* and shows the assortment of Bi crystals on the surface up to 10 nm in height and up to 1 μm in lateral size. As θ_{Bi} is increased further to 12.5 ML, as well as the annealing time to 2 h (Fig. 4, *h*), the crystals grow even larger: up to 80 nm in height and up to 5 μm laterally.
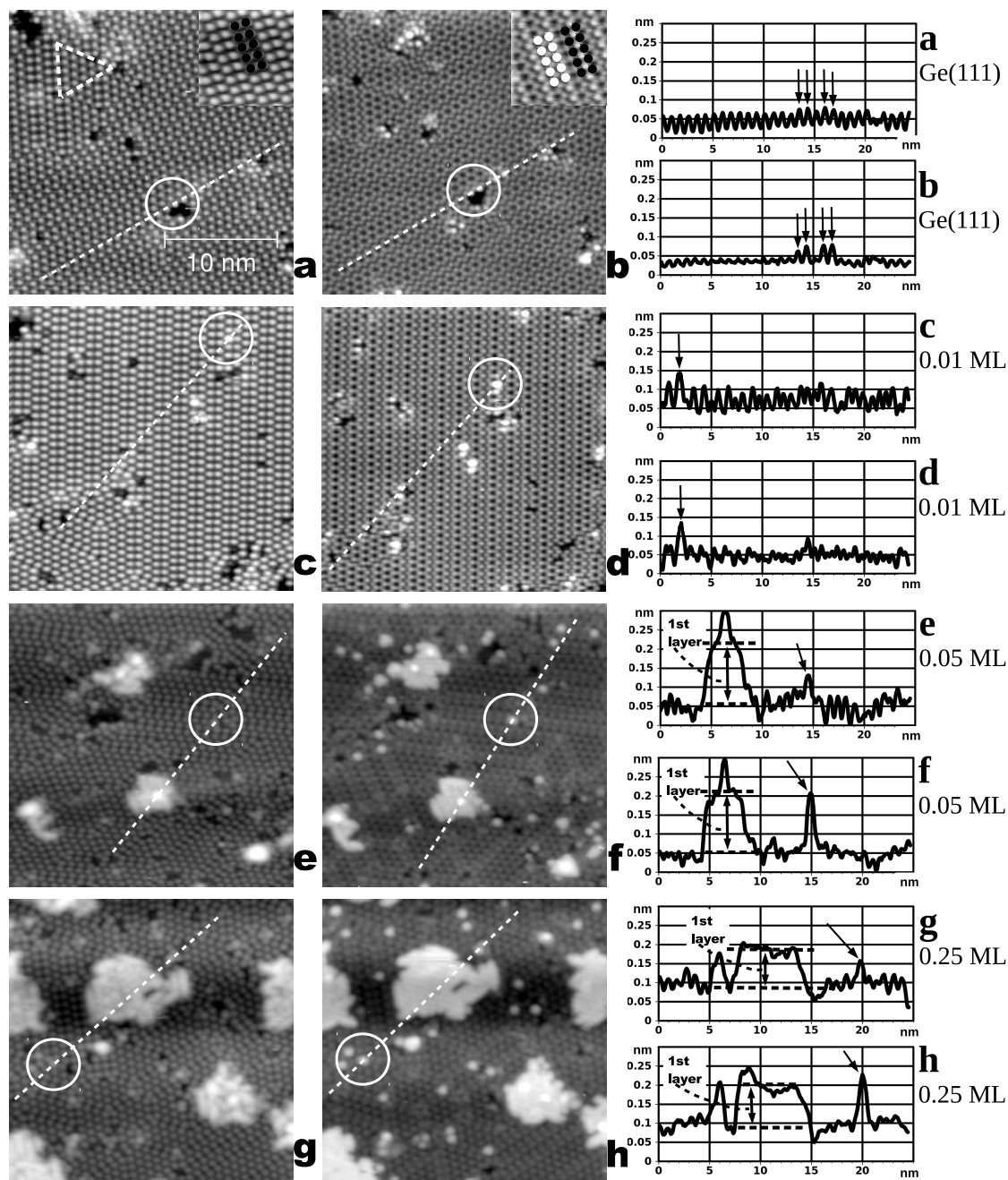
The tendency demonstrated by the sequence of images in Fig. 4, *d–h* is clearly the opposite one to that in Figs. 1, *e–f*; 2, *a–f*. Namely, increasing θ_{Bi} = up to 12.5 ML in the annealed film leads to the surface roughening instead of the flattening for the as-deposited film. Obviously, this roughening is caused by the surface diffusion of Bi on the top of the wetting layer during the annealing. The resulting films in Fig. 4, *g–h* consist of a variety of nanocrystals, their sizes ranging from dozens to thousands of nm. Therefore, the annealing of Bi films at 450 K in the UHV environment, with a nominal thickness of the order of 10 ML, leads to their microstructuring.

The scale of Fig. 4 is too rough for the adequate perception of essential details in panels *a-b* (submonolayer Bi films after the annealing at 450 K). Thus, in Fig. 5, we present a set of 25 nm × 25 nm STM images with atomic resolution, where the same surface area of every specimen is imaged both in empty and occupied states). For reference purposes, Fig. 5, *a–b* shows the pure Ge(111) substrate, on which the imaged area was specially selected to include a large number of surface defects. In this way, we observe simultaneously the regular c(2 × 8) reconstruction (occupying the majority of the surface area), small patches of the (2 × 2) reconstruction (enclosed by white dashed triangle), as well as various types of single atomic and grouped surface vacancies. The basic Ge(111)-
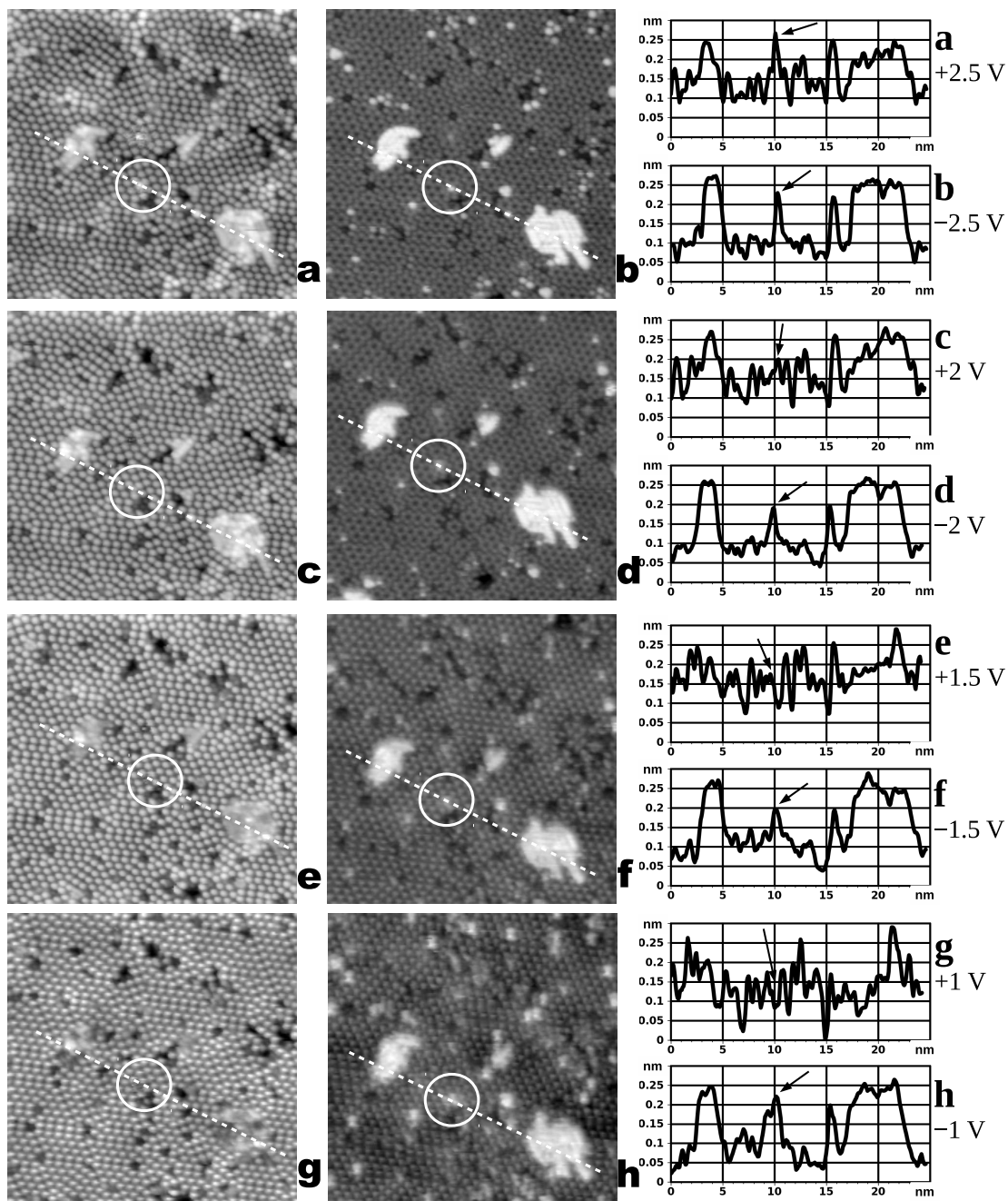
c(2 × 8) structure consists of the so-called adatoms and restatoms, which are both seen in occupied states (Fig. 5, *b*), while only adatoms are visible in empty states (Fig. 5, *a*) [26]. The insets in the upper right corners of Fig. 5, *a, b* show 6 nm × 6 nm STM images of an ideal c(2 × 8) reconstruction in empty and occupied states, correspondingly, where the black solid circles designate adatoms, while white solid circles designate restatoms.

On a clean germanium surface, some adatoms or restatoms can be brighter than the surrounding if they find themselves in vicinities of defects, such as the vacancies or domain boundaries. In the constant current mode of STM operation, the higher brightness means the higher local density of states in either empty or occupied electronic states. Different STM images in Fig. 5 use different gray scales to emphasize the visual perception of essential details. However, the height-to-distance cross-sections use similar vertical and horizontal scales. In this way, the height differences can be compared among all cross-sections, but not the absolute heights, as the cross-sections do not share any common reference height point. In Fig. 5, *a, b*, we identify four Ge atoms, which are adjacent to a group vacancy and have a substantialy higher brightness in the occupied states (cross-section 5, *b*), but look almost the same as the surrounding in the empty states (cross-section 5, *a*). They are marked by black arrows on the cross-sections, and the corresponding locations are enclosed by white circles on the images.

The specimens with various submonolayers θ_{Bi} were annealed at 450 K for half an hour in the UHV environment. In Fig. 5, *c–d*, at θ_{Bi} = 0.01 ML, some atoms amidst an atomically flat terrace are clearly brighter than their surrounding both in the images of empty and occupied states. Such atoms are also present in Fig. 5, *e–h* for θ_{Bi} = 0.05 ML and θ_{Bi} = 0.25 ML, where the first-layer Bi islands are already formed. They are marked with black arrows on the cross-sections, and their corresponding locations are designated by white circles on the STM images. The objects in question are always substantially brighter than the surrounding Ge atoms in the images of occupied states (Fig. 5, *b, d, f, h*). But, for the images of empty states, the same is true only on the surface, where Bi is present (Fig. 5, *c, e, g*). A thorough analysis of Fig. 5, *a* and many other images of the pure Ge(111) has not revealed any atomic scale objects within the outermost surface layer, which are re-

Fig. 5. Evolution of annealed submonolayer Bi films on Ge(111) as θ_{Bi} is varied from 0 to 0.25 ML. All STM images are 25 nm × 25 nm, the images within pairs *a–b, c–d, e–f* and *g–h* were obtained on the same surface areas of the corresponding specimens (small shifts are due to residual thermal drift). Panels *a, c, e* and *g* contain the images of empty states obtained with +2 V specimen bias voltage; panels *b, d, f* and *h* contain the images of occupied states obtained with −2 V specimen bias voltage. The right-most column contains cross-sections, which were obtained as height vs distance curves along white dashed lines within corresponding images. Every cross-section is labeled by the same letter as the image, in which it was taken, and by the deposited amount of Bi (in monolayers). The cross-sections are presented on similar vertical and horizontal scales to allow the comparison of height differences (no common height reference point). See the text for the discussion

Fig. 6. Voltage-dependent STM imaging of Bi/Ge(111): incorporated vs on-top. All STM images are 25 nm × 25 nm and show the same surface area (only small lateral shifts are present due to the thermal drift) of the specimen with $\theta_{Bi} = 0.05$ ML, after the annealing at 450 K for 30 min. The specimen bias voltages are: *a*) +2.5 V; *b*) −2.5 V; *c*) +2 V; *d*) −2 V; *e*) +1.5 V; *f*) −1.5 V; *g*) +1 V; *h*) −1 V. The right-most column contains cross-sections, which were obtained as height vs distance curves along white dashed lines within corresponding images. The cross-sections are labeled by the same letters as the corresponding images, they do not share any common height reference point. An individual Bi atom incorporated into the uppermost atomic layer of the substrate is present at a lateral coordinate of ∼10 nm in every cross-section and is designated by black arrows and white circles

liably imaged as brighter than the surrounding atoms at the ± 2 V specimen bias voltage. This fact allows us to assign them tentatively to individual Bi atoms, which substitute individual Ge adatoms of the intrinsic reconstructed surface, hence, incorporated Bi atoms. In addition, Fig. 5, *e–h* allows for the distinction between the incorporated Bi atoms and the first layer Bi atoms, while the latter were thoroughly investigated in our previous work [7]. After the comprehensive analysis of a large set of STM images of as-deposited Bi films, no incorporated Bi atoms were found. Therefore, we are able to conclude that the incorporation of Bi atoms into Ge(111)-c(2 × 8) does not take place at 300 K and requires the thermal activation at 450 K in order to proceed.

The most general distinction criterion can be formulated in the following way: the individual atoms, which appear brighter than the surrounding germanium substrate both in empty and occupied states at high enough bias voltages, but are still lower in height than the first-layer Bi islands at least for some bias voltage, should be considered as Bi atoms substituting individual Ge adatoms of the reconstructed Ge(111) surface. In other words, these are the individual Bi atoms being incorporated in-registry into the uppermost atomic layer of the substrate. This distinction principle is further illustrated by Fig. 6, where the annealed specimen with $\theta_{\mathrm{Bi}} = 0.05$ ML is shown at various specimen bias voltages. Figure 6, *a–h* shows STM images of the same area on the specimen, containing both the incorporated Bi atoms and the first-layer Bi islands. In Fig. 6, *a–b*, a bias of ± 2.5 V is required to unambiguously identify the incorporated Bi atom: on all the cross-sections of Fig. 6, it is designated by a black arrow at a lateral coordinate of ~ 10 nm (the corresponding location is encompassed by white circles on the images). The ± 2.5 V bias is somewhat higher than ± 2 V, which was the case in Fig. 5. Such difference can be attributed to different conditions of the STM probe tip, causing the near-surface tip-induced band bending [27] to a different degree in the measurements of Fig. 5 vs Fig. 6.

As the absolute value of bias voltage is lowered from ± 2.5 V (Fig. 6, *a–b*) to ± 2 V (Fig. 6, *c–d*), ± 1.5 V (Fig. 6, *e–f*), and ± 1 V (Fig. 6, *g–h*), the given incorporated Bi atom continues to be imaged brighter than the surrounding substrate in the occupied states but still less bright than the first-layer Bi islands (Figs. 6, *d, f, h*). Simultaneously, this atom

in the empty states looks similar to the germanium surrounding in Fig. 6, *c* and even darker than the surrounding in Fig. 6, *e–g*. This latter tendency, namely the local density of empty states being lower than for germanium substrate as the tunneling proceeds closer to the Fermi level, is very similar to what was reported in our previous work [7] for the Bi species situated directly on the top of Ge(111). The same is, of course, observed in Fig. 6, *e–g* for the first-layer Bi islands, also contained within cross-sections. Figure 6, *g* is of particular interest since it, if viewed on it own, would not suggest the presence of any adsorbate on the surface. This means that the Bi adsorbates possess an extremely low density of empty states within 1 eV from the Fermi level as compared to the surrounding substrate. Knowing the locations of Bi islands from the images of occupied states, a detailed examination of these locations in Fig. 6g reveals atomic structures similar to what is observed on the surrounding pure germanium areas. Therefore, the islands do not contribute to the tunneling current and become "transparent" in the sense that the underlying substrate is imaged instead of them.

5. Discussion

The results presented above, as well as in our previous work [7], allow us to build a complete picture of how the growth of Bi proceeds on Ge(111)-c(2×8) at 300 K and to compare it with a closely related Si(111)-(7×7) substrate. Our results for growth stage I, namely from 0 to 3.5 ML, demonstrate unambiguously that the initial growth proceeds in the Vollmer–Weber mode (see Fig. 3). The culmination of this stage is the uniform 3D nanostructuring of the film in the form of Bi nanocrystals with heights of the order of 1 nm and lateral sizes of the order of 10 nm (see Fig. 1). It is important that these Bi nanocrystals are laterally isolated entities and, therefore, can serve as a homogeneous array of quantum dots for practical applications in nanoelectronics, photonics, *etc.*

The Bi nanocrystals observed by us are predominantly of rectangular shape (in projection onto the substrate plane), which is very similar to the nanocrystals of the pseudocubic Bi allotrope, as predicted theoretically and observed experimentally on the Si(111) substrate for the same film thickness range [10–12, 28]. The difference between Bi/Si(111) and Bi/Ge(111) is the earlier onset (in terms of θ_{Bi}) of

the growth of pseudocubic nanocrystals. Namely, the wetting layer on Si(111) consists of clusters, which are readily formed at the Bi deposition onto Si(111)-(7×8) [10, 12], whereas an almost epitaxial first atomic layer is formed initially on Ge(111)-c(2×8) [7] and only then do the small 3D clusters start to build up (see Figs. 1 and 3).

The {012} surface orientation of the pseudocubic Bi allotrope in the Bi/Si(111) system is characterized by double layers of Bi atoms with strong covalent bonds within the double layer and weak van der Waals bonds between the neighboring ones [10–12, 28]. This leads to the pronounced stability of double layers, dictating the discrete values of nanocrystals' heights (relative to the wetting layer) as multiples of the {012}-oriented double layer thickness (0.66 nm). In the present work, at the beginning of growth stage II, Bi film's coarsening is observed, and the discrete heights of Bi nanocrystals become evident (see Fig. 2). The first discrete height measures 0.65 nm from the top of the wetting layer, which is in very good agreement with the {012} double layer. The second value is 1.25 nm, giving an increment by 0.6 nm, which is slighty lower than the purely geometrical 0.66 nm reference value. This deviation may be caused by the effects of the electronic density of states, leading to a somewhat lower thickness of the second double layer, as measured from the STM height-distance profile. In-line with this tendency is the next increment of 0.59 nm, which may be assigned to the third double layer.

During growth stage II, we observe the formation of a continuous Bi film. At $\theta_{Bi} = 10$ ML, the surface unit cell is rectangular with 0.49 nm and 0.43 nm in-plane periodicities (see Fig. 3). They are in fairly good agreement with 0.47 nm and 0.45 nm in-plane periodicities of the {012}-oriented pseudocubic Bi allotrope in the Bi/Si(111) system [10–12, 28], while the discrepancy is due to the thermal drift and calibration issues. Such rectangular unit cell together with Bi nanocrystals' discrete heights substantiate the assumption about the growth of a pseudocubic Bi allotrope on the Ge(111) substrate similarly to the case of Si(111). The pseudocubic crystalline structure of Bi on Si(111) is predicted and observed to be stable only below some critical thickness, above which it transforms into the rhombohedral structure inherent to the bismuth bulk [10–12, 28]. The data obtained in this work (see Fig. 3) at $\theta_{Bi} = 15$ ML demonstrate

a triangular lattice with the 0.45-nm periodicity at the end of growth stage II in excellent agreement with the 0.45-nm in-plane periodicity of the bulk-like Bi(001). In addition, this transformation is fully in-line with the results for the Bi/Ge(111) system reported by other authors [20].

An important new observation of our present work is that the transformation between the pseudocubic allotrope and the rhombohedral bulk-like crystalline structure is accompanied by a dramatic flattening of the Bi film on Ge(111). Such flattening is an unexpected departure from the standard Vollmer–Weber growth mode scenario and can be utilized in those practical applications, where ideal film's surface is of primary importance. A similar smoothing of Bi film's morphology was observed on the Si(111) substrate [11]. Additionally, the flattening of substantially thicker (56 ML) Bi(001) films was previously observed on the Si(111) substrate, but only as a result of the annealing above 350 K [29]. At this thickness, there were no traces of the pseudocubic Bi allotrope, and the flattening was caused exclusively by the increased surface mobility of Bi atoms (pre-melting).

It is important to compare our real space STM results with the studies of the Bi/Ge(111) system by means of the electron diffraction. The most comprehensive investigation of the Bi film growth on Ge(111) by means of the low energy electron diffraction (LEED) was performed by Hatta *et al.* [20]. Their LEED results are completely in line with all known STM data, showing a gradual transition from the {012}-oriented pseudocubic Bi allotrope to a rhombohedral Bi(001) film in the thickness range from 6 to 10 ML. The LEED technique also provides information, which is inaccessible for STM. In particular, the c(2×8) reconstruction of the substrate vanishes under the bismuth wetting layer [20], being in strong contrast to the case of the Si(111) substrate, the latter retaining its (7×7) reconstruction below the growing film [11]. Otherwise, there is a qualitative agreement between the LEED data on the growing Bi film on Ge(111) and Si(111) substrates.

Some LEED data on the Bi/Ge(111) system were also obtained in our work group by other authors [30]. They confirmed the disappearance of the spots attributed to the c(2×8) reconstruction within the LEED pattern of the 1-ML Bi film deposited at 300 K. Only the bulk-like (1×1) spots of Ge(111) were present on such specimen, but even they have dis-

appeared after the deposition of a 10-ML Bi film, the latter being thick enough to block the escape of low-energy electrons from the specimen. In the same work, the effects of the annealing temperature variation were investigated by means of Auger electron spectroscopy (AES) for the 10-ML film grown at 300 K. The AES Bi(NOO, 102 eV)/Ge(MNN, 52 eV) peak ratio decreased dramatically after 450 K, standing in perfect agreement with the morphological changes of the Bi film after such annealing observed by us in the present work. Namely, the thermally activated redistribution of bismuth on the substrate leads to film's coarsening and thus increases the substrate area, where Auger electrons originating from the germanium substrate can escape into the vacuum.

6. Conclusions

Thus, the results of detailed STM studies of the Bi growth on Ge(111)-c(2×8) at 300 K up to 15 ML indicate the Vollmer–Weber type of growth. We have identified the growth regime for the effective 3D nanostructuring of a Bi film with the sizes of nanocrystals up to 10 nm and up to several dozen nm, as well as for the effective flattening of the film due to pseudocubic Bi allotrope's transition to the rhombohedral bulk Bi crystalline structure. For the films annealed at 450 K in UHV, we have identified regimes for the 2D nanostructuring with typical lateral sizes up to 10 nm, as well as for the 3D microstructuring. Moreover, we have shown that the thermal stimuli induce the incorporation of Bi atoms into the topmost Ge substrate layer and have developed a reliable criterion for their recognition.

1. Ph. Hofmann, Progr. in Surf. Sci. **81**, 191 (2006).
2. Yu.M. Koroteev, G. Bihlmayer, J.E. Gayone *et al.*, Phys. Rev. Lett. **93**, 046403 (2004).
3. Yu.M. Koroteev, G. Bihlmayer, E.V. Chulkov *et al.*, Phys. Rev. B **77**, 045428 (2008).
4. I. Gierz, T. Suzuki, E. Frantzeskakis *et al.*, Phys. Rev. Lett. **103**, 046803 (2009).
5. S. Hatta, T. Aruga, Y. Ohtsubo *et al.*, Phys. Rev. B **80**, 113309 (2009).
6. Y. Ohtsubo, S. Hatta, K. Yaji *et al.*, Phys. Rev. B **82**, 201307(R) (2010).
7. A. Goriachko, P.V. Melnik, A. Shchyrba *et al.*, Surf. Sci. **605**, 1771 (2011).
8. N. Ballav, C. Wäckerlin, D. Siewert *et al.*, J. of Phys. Chem. Lett. **4**, 2303 (2013).
9. W. Hieringer, K. Flechtner, A. Kretschmann *et al.*, J. of the Amer. Chem. Soc. **133**, 6206 (2011).
10. J.T. Sadowski, T. Nagao, S. Yaginuma *et al.*, J. of Appl. Phys. **99**, 014904 (2006).
11. T. Nagao, J.T. Sadowski, M. Saito *et al.*, Phys. Rev. Lett. **93**, 105501 (2004).
12. Y. Oh, J. Seo, H. Suh *et al.*, Surf. Sci. **602**, 3352 (2008).
13. K. Miki, J.H.G. Owen, D.R. Bowler *et al.*, Surf. Sci. **421**, 397 (1999).
14. M. Naitoh, M. Takei, S. Nishigaki *et al.*, Surf. Sci. **482-485**, 1440 (2001).
15. J.H.G. Owen, D.R. Bowler, K. Miki *et al.*, Surf. Sci. **596**, 163 (2005).
16. A.G. Mark, J.A. Lipton-Duffin, J.M. MacLeod *et al.*, J. of Phys.: Cond. Matter **17**, 571 (2005).
17. H.K. Louwsma, H.J.W. Zandvliet, B.A.G. Kersten *et al.*, Surf. Sci. **381**, L594 (1997).
18. C. Cheng and K. Kunc, Phys. Rev. B **56**, 10283 (1997).
19. Y. Ohtsubo, S. Hatta, M. Iwata *et al.*, J. of Phys.: Cond. Matter **21**, 405001 (2009).
20. S. Hatta, Y. Ohtsubo, S. Miyamoto *et al.*, Appl. Surf. Sci. **256**, 1252 (2009).
21. I.V. Lyubinetsky, P.V. Melnik, N.G. Nakhodkin *et al.*, Vacuum **46**, 219 (1995).
22. R.S. Becker, B.S. Swartzentruber, J.S. Vickers *et al.*, Phys. Rev. B **39**, 1633 (1989).
23. E.S. Hirschhorn, D.S. Lin, F.M. Leibsle *et al.*, Phys. Rev. B **44**, 1403 (1991).
24. G. Lee, H. Mai, I. Chizhov *et al.*, J. of Vacuum Sci. and Techn. A **16**, 1006 (1998).
25. G. Lee, H. Mai, I. Chizhov *et al.*, Surf. Sci. **463**, 55 (2000).
26. I. Razado-Colambo, J. He, H.M. Zhang *et al.*, Phys. Rev. B **79**, 205410 (2009).
27. R.M. Feenstra, S. Gaan, G. Meyer *et al.*, Phys. Rev. B **71**, 125316 (2005).
28. M. Saito, T. Ohno, T. Miyazaki, Appl. Surf. Sci. **237**, 80 (2004).
29. S. Yaginuma, T. Nagao, J.T. Sadowski, Surf. Sci. **547**, L877 (2003).
30. M.G. Nakhodkin and M.I. Fedorchenko, Visn. Kyiv. Univ. Ser. Fiz. Mat. **4**, 236 (2010).

А. Горячко, А. Щирба,
П.В. Мельник, М.Г. Находкін

РІСТ ВІСМУТУ НА Ge(111): ЕВОЛЮЦІЯ
МОРФОЛОГІЇ ВІД НАНОКРИСТАЛІВ ДО ПЛІВОК

Р е з ю м е

Досліджено ріст надтонких плівок вісмуту до 15 атомарних шарів на атомарно чистій підкладці Ge(111)-c(2×8) при 300 К методом надвисоковакуумної скануючої тунель-

ної мікроскопії до та після відпалу при 450 К. Спостерігався такий діапазон морфологій вісмутового адсорбату: окремі атоми, двовимірні наноострівці, тривимірні нанокристали, мікрокристали, а також атомарно гладка плівка. Тривимірна (3D) наноструктуризація досягається в процесі росту плівки за сценарієм Вольмера–Вебера до 10 атомних шарів. За подальшого росту від 10 до 15 атомарних шарів відбувається згладжування поверхні плівки. Після відпалу субмоношарових плівок спостерігалися окремі атоми Bi, вбудовані у зовнішній атомарний шар підкладки Ge(111), а також двовимірні острівці першого атомарного шару плівки (2D наноструктурування). Плівки більшої товщини зазнавали розрихлення внаслідок відпалу і складались із низки нано- та мікрокристалів вісмуту.